Transposon expression in the *Drosophila* brain is driven by neighbouring genes and diversifies the neural transcriptome

Christoph D. Treiber* & Scott Waddell*
Centre for Neural Circuits and Behaviour, University of Oxford, Tinsley Building, Mansfield Road, Oxford OX1 3SR, UK
*Corresponding authors.
Email: christoph.treiber@cncb.ox.ac.uk, scott.waddell@cncb.ox.ac.uk

Abstract

Somatic transposition in neural tissue could contribute to neuropathology and individuality, but its prevalence is debated. We used single-cell mRNA sequencing to map transposon expression in the *Drosophila* midbrain. We found that neural transposon expression is driven by cellular genes. Every expressed transposon is resident in at least one cellular gene with a matching expression pattern. A new long-read RNA sequencing approach revealed that coexpression is a physical link in the form of abundant chimeric transposon-gene mRNAs. We identified 148 genes where transposons introduce cryptic splice sites into the nascent transcript and thereby produce many additional mRNAs. Some genes exclusively produce chimeric mRNAs with transposon sequence and on average transposon-gene chimeras account for 20% of the mRNAs produced from a given gene. Transposons therefore significantly expand the neural transcriptome. We propose that chimeric mRNAs produced by splicing into polymorphic transposons may contribute to functional differences between individual cells and animals.

Introduction

Transposons comprise almost half of every eukaryote genome (Britten and Kohne, 1968; International Human Genome Sequencing Consortium et al., 2001; Ketchum et al., 2000) and their mobilization in the germline contributes to chromosome evolution. Non-heritable *de novo* transposon activity in neural tissue has been proposed to contribute to functional heterogeneity in the brain and to neurological disease (Baillie et al., 2011; Coufal et al., 2009; Evrony et al., 2012; Kazazian, 2011; Muotri et al., 2005). However, it is difficult to faithfully map rare *de novo* transposon insertions using whole-genome DNA sequencing (Baillie et al., 2011; Evrony et al., 2012, 2016; Perrat et al., 2013; Treiber and Waddell, 2017; Upton et al., 2015). A growing number of studies have therefore correlated the development of neurodegeneration in animal models with changes in transposon expression (Guo et al., 2018; Krug et al., 2017; Li et al., 2013; Li et al., 2012; Sun et al., 2018). Using expression as a proxy for mobility could be misleading because high-level transposon expression does not appear to result in elevated *de-novo* somatic transposition in the brain (Evrony et al., 2012, 2016; Treiber and Waddell, 2017). It is therefore important to understand what controls the expression of transposon-derived sequences in the brain and whether their elevated expression relates to neural function.

An early study of the human LINE-1 (L1) promoter demonstrated that its activity was heavily influenced by flanking cellular sequences, and concluded that expression of a given L1 depended on its location in the genome (Lavie et al., 2004). Such a locus specific model could more generally explain the apparent cell-type restricted nature of transposon expression and mobilization in the brain. So far, studies of somatic transposon expression have either focused on single transposon families or have been based on bulk sequencing of tissues or cultured cells (Chung et al., 2019; Faulkner et al., 2009; Li et al., 2013; Philippe et al., 2016; Rangwala et al., 2009). However, answering this question on a brain- and genome-wide scale requires a means to relate the cellular expression of each transposon in the genome to that of their neighbouring genes. Recent technical developments in whole-genome DNA sequencing and high-throughput single-cell transcriptomics of complex tissues now make this possible (Macosko et al., 2015).

Here we used single-cell transcriptomics to map transposon expression to individual cells in the *Drosophila* midbrain. We found that many transposons are expressed with cell-specificity that is often highly correlated to that of a neighbouring gene. A more detailed analysis revealed that >90% of transposon expression can be linked to co-expression with their host gene, indicating that these genes are the main driver of somatic transposon expression. Long-read sequencing showed that the transposon and neighbouring gene are alternatively

spliced together becoming part of the same chimeric mRNAs. Sometimes all mRNAs produced from a particular gene in which a transposon resides include transposon sequence. Therefore, transposons produce genome-wide diversification of cellular transcripts. Analysis of sequencing data produced from other fly strains demonstrated large differences in their chimeric transcriptomes. Inter-strain and individual differences in transposon complement therefore constrain the cellular specificity and likelihood of transposon-directed pathology.

Results

Single-cell transcriptomics reveals cell-type restricted transposon expression

The *Drosophila* genome contains 112 families of transposons and the number of an individual types varies from a few to hundreds of copies (Kaminker et al., 2002). Conventional single-cell RNAseq (scRNAseq) analysis pipelines typically discard sequencing reads that align to multiple genomic loci and so they overlook transposon expression. We therefore devised an analysis pipeline to map the expression of all transposons within scRNAseq data. We masked all repetitive sequences in the reference genome and then added a single copy of the consensus sequence for every known transposon to the masked genome. In essence this produces a *Drosophila* reference genome with one copy of each type of transposon. We first used this modified reference genome to map transposon expression onto single cells of the midbrain in a fly strain expressing mCherry in αβ Kenyon cells (KCs) of the mushroom body (MB); from here called αβCherry flies. We found evidence for expression of both the sense and the antisense strand of most transposons, which comprised 76.2 and 23.8% (+/- 1.7% SD) of all transposon expression, respectively (Figure 1 – figure supplement 1). We first performed principal component decomposition of cellular genes and clustered cells from the midbrain by constructing a k-Nearest-Neighbour graph on the Euclidean distances in the PCA space, optimizing the modularity using the Louvain algorithm (Butler et al., 2018). This analysis grouped cells into many discrete clusters. We next assigned many of these clusters to cell types in the midbrain using the expression patterns of known marker genes (Croset et al., 2018) (Figure 1a). Displaying the expression of individual types of transposons on the cluster plot revealed that some transposons are up-regulated in specific cell types. For example, the long-terminal repeat (LTR) retrotransposons COPIA and NOMAD showed elevated expression in the αβ, α´β´ and γ Kenyon Cells (KCs) classes (Figure 1b, first graph) and α´β´ KCs (Figure 1c, first graph), respectively. Other LTR retrotransposons such as MICROPIA were upregulated in the ellipsoid body (Figure 1d, first graph) whereas BLOOD and 412 were higher in glia (Figure 1e,f, first graphs).

Transposon expression correlates with that of cellular genes they are inserted within.

Transposons could be elevated in specific cell types because they are inserted in genes that are highly expressed in the same cells. To test this hypothesis, we re-used our previously published high-coverage gDNA sequence of αβCherry flies. We mapped all the germline transposon insertions in these flies using TEchim, a new custom-built transposon analysis program. TEchim first generates long nucleotide contigs from either gDNA or cDNA sequencing reads, then creates in-silico paired-end reads and screens them for cases where one in-silico end maps to a cellular gene and the mate read maps to a specific transposon.

Since these paired-end reads are derived from contiguous sequences, TEchim permits one to subsequently refer back to the original long reads to determine the precise nucleotide sequence of the transposon-gene breakpoints. Using TEchim, we found copies of COPIA, NOMAD, MICROPIA, BLOOD and 412 inside the genes *twin-of-eyeless* (*toy*), *mushroom-body expressed* (*mub*), *Rhodopsin-7* (*Rh7*), *CG32521* and *tequila* (*teq*), respectively. The expression of each of these genes mirrored the expression pattern of the transposon they harboured (Figure 1b-f, second graphs). The expression of these transposons in the brain of αβCherry flies therefore appears to be driven by their relevant host genes.

We next tested whether all transposons exhibit patterned expression throughout the midbrain. We re-clustered the single-cell data of the fly using only transposon expression. This generated 78 cell clusters that mostly contained cells from all 8 biological replicates in the data (Figure 1g, Figure 1 – figure supplement 2). This result suggests that transposon expression is stereotyped across samples derived from different flies collected from the same strain. We then analysed the expression of cellular genes across the transposon clusters and found many clusters also preferentially expressed certain genes. For example, the cluster of cells expressing the LTR of STALKER2 was enriched for cells that also expressed the *Hsp70Bc* gene (Figure 1h), and cells in the DOC-positive cluster showed increased expression of *Furin1* (*Fur1*). By referring back to the gDNA, we found that αβCherry flies harbour a copy of STALKER2 within *Hsp70Bc* and a copy of the LINE-like DOC element inside *Fur1*. Again, these data suggest that expression of STALKER2 and DOC is driven by a neighbouring gene.

Quantitative analysis reveals high fidelity transposon-gene co-expression

Our gDNA analysis also revealed many transposon insertions inside genes that were more broadly expressed across the brain. In total, we identified 1952 germline transposon insertions within genes. Of these, 881 cases were inserted in the sense direction to the open reading frame of the gene and 1071 were in the antisense orientation (Supplementary Table 1). To quantify the correlated expression of transposons and cellular genes we devised a method based on the established Hardy-Weinberg principle for quantifying linkage equilibrium of two alleles in population genetics (Lewontin and Kojima, 1960) (Figure 2a). We first binarized our scRNAseq data to generate the equivalent of bi-allelic traits in a population. We then calculated the proportion of cells expressing a specific transposon, multiplied it by the proportion of cells expressing a certain gene, and then subtracted this value from the proportion of cells that expressed both the transposon and the gene. We termed this value the Coexpression Disequilibrium, CD. We also normalized these CD values to account for the variable abundance of each transposon and gene in every

transposon-gene pair and repeated the analysis for all transposon-transposon and gene-gene pairs. These normalized values were then ranked within each of the 8 biological replicates. P-values were corrected for multiple comparisons and describe the probability that a transposon-gene pair would have such a highly ranked CD value across multiple replicates if they were expressed independently.

We combined the list of all germline transposon insertions in αβCherry flies with the scRNA seq data generated from the same population of flies and calculated the CD values between every transposon and the gene in which it was inserted. We tested every transposon that contributed at least 0.1% of the overall transposon expression in our midbrain αβCherry fly samples. This cut-off left 59 different transposons, 34 of which were expressed in both the sense- and the antisense direction, 22 only in sense, and 3 only in antisense (Figure 2b, Supplementary Table 2). For 56 of these transposons we found at least one copy inside a gene that exhibited a correlated expression pattern (Benjamini-Hochberg corrected p-val >0.05). For those cases where the transposon was inserted in the same orientation as the transcription unit of the gene the expression of the sense strand of the transposon correlated to that of the gene. In contrast, the antisense strand of reverse orientation transposons was correlated with the host gene. Importantly, the average number of correlated genes for each transposon was significantly less if equivalent values were calculated using random assignment of transposons to host genes (Figure 2c). These analyses therefore demonstrate that the genomic locus strongly influences the expression patterns of almost all transposons in the fly brain. We did not identify a neighbouring gene with a correlated expression pattern for the transposons TART-A, P-element and HMSBEAGLE. This is expected for TART-A, which is a telomeric retrotransposon, and for P-element, which is a remnant of transgenic intervention in αβCherry flies. It is conceivable that the HMSBEAGLE retrotransposon is the only element that is expressed independently of a cellular gene. However, despite our high coverage sequence of αβCherry flies we may have missed a germline HMSBEAGLE insertion that sits near a gene that is driving its expression.

Transposons are exonised into cellular mRNAs

Recent work has shown that mRNAs from the *Arc* gene contain transposon-like sequence in the coding sequence and 3′ UTR (Pastuzyn et al., 2018; Zhang et al., 2015). We therefore tested whether chimeric mRNAs might occur more broadly and extend to all transposons. We extracted mRNA from αβCherry fly heads and generated 250 basepair long reads which were screened using TEchim for chimeric reads. We also incorporated a function in TEchim that maintains strand-specificity of the input reads which enabled us to unambiguously assign chimera to cellular genes. This analysis revealed that a large number of transposons

inside introns lead to the formation of chimeric mRNAs. In total, we found chimeric mRNA from 887 transposon insertions (Figure 3a, Supplementary Table 3). Chimera included sequences from LTR, LINE-like and DNA transposons attached to mRNAs from genes involved in a broad range of biological processes. For example, we found sequence from the LTR-retrotransposon GYPSY in transcripts of the ubiquitin gene *Ubi-P5E* and of the neuron specific ubiquitin ligase *highwire* (*hiw*), the non-LTR element DOC in *Fur1*, encoding a synaptic membrane bound protease, and the TIR element HOBO attached to transcripts from *Shaker*, which encodes a voltage-gated potassium channel (Izquierdo, 1994; Kaplan and Trout, 1969; Roebroek et al., 1991; Wan et al., 2000).

Previous studies of chimeric sequencing reads have established that *in vitro* amplification of genetic material often leads to chimeric amplification artefacts (Evrony et al., 2016; Treiber and Waddell, 2017). It was thus important to account for similar errors in our data. We therefore calculated the rate of these artefacts in our mRNA data by selecting 10 sets of 167 exons (with each set providing a number of sequences corresponding to the 112 different transposon types and 55 LTRs) with matching expression levels in the brain. These exons lack the ability to relocate in gDNA so we refer to them as immobile genetic elements (IGEs). Since IGEs should only occur as single copies in the gDNA from αβCherry, chimeric reads between IGEs and other genes most likely represent amplification artefacts. We found the rate of generating IGE chimeras was directly correlated to the expression level of the IGE and the gene that it formed a chimeric molecule with. Critically, the IGE chimera rate was substantially lower than that of chimera formed between genes and transposons. We therefore used the rate of IGE chimera to filter the transposon chimera detected using TEchim, defining a false discovery rate (FDR) of 0.1% (Figure 3b, Supplementary Table 3). All examples of chimeric transcripts that are presented in detail in this study have supporting evidence that exceeds this FDR.

LTR retrotransposon expression is predominantly non-autonomously

Given that transposon expression was highly correlated with at least one neighbouring gene, we hypothesized that all transposon expression in the brain might occur as co-expression with cellular genes. To test this, we focused on LTR retrotransposons. We quantified the number of reads that spanned an LTR-gene breakpoint, and compared it to the number of reads that crossed the LTR-transposon breakpoint within the transposon (Figure 4a). Autonomously expressed, full-length transposons only generate the latter type of read, whilst non-autonomous expression should generate both kinds of reads, at varying proportions. We found that around 95% of the highly expressed LTR transposons produced a roughly equivalent number of gene-transposon and LTR-transposon reads, suggesting that LTR

transposons are expressed as chimeras with cellular genes, rather than being autonomously expressed (Figure 4b, Supplementary Table 4).

Many transposons introduce cryptic alternative splice-sites into cellular genes

Given the abundance of reads that span a gene-transposon breakpoint, we next investigated the structure of these transcripts in more detail. Our transposon mapping identified 887 loci with a germline transposon insertion in the intron of a gene. For each of these we found mRNA molecules where one section mapped to the beginning or end of the transposon and the other section corresponded to the flanking intronic sequence. These reads could represent nascent unspliced chimeric pre-mRNAs from which transposon-derived sequence could be removed by splicing to yield intact host mRNAs, and full-length transposon sequences. However, we also found 148 examples where breakpoint-spanning reads indicate that specific sections of transposon sequence are spliced into host-gene transcripts (Supplementary Table 5).

Analysis of the breakpoints inside transposons at these 148 sites revealed that chimera are formed at conserved locations in each type of transposon. For example, in cases where an antisense ROO resided within an intron, we found transcripts where the 3´-end of an upstream exon had formed a new phosphate bond to a section of ROO at positions 5460 and 2094 at 19 and 3 different genomic loci, respectively, and also at several additional breakpoints with lower frequency (Figure 5a,b). In addition, we identified transcripts where sections of ROO were bound to the 5´-end of a downstream exon. We found breakpoints at position 5191 from 24 genes, two at 2783, and several others at unique positions (note that the numbering runs backward because it relates to the forward orientation of ROO). Whereas intronic antisense ROO provides gene-transposon breakpoints for 28 exons, and transposon-gene breakpoints for 33, intronic sense ROO only introduced 4 and 1 (Figure 5c). Similarly, the LTR BLOOD also introduced more breakpoints when it was inserted in the antisense orientation relative to the host gene (14 vs. 6, Figure 5d,e).

We screened the transposon sections around breakpoints for consensus splice- acceptor (SA) and donor (SD) sequence motifs and found many cases where the gene-to-transposon chimera had been formed at SA consensus motifs, and transposon-to-gene chimera at SD motifs (Stephens and Schneider, 1992) (Figure 4 – figure supplement 1, Supplementary Table 6). For example, all breakpoints in antisense BLOOD that were formed with more than one exon were precisely located at the predicted SA and SD splice site (Figure 5d). Interestingly, we did not find a consensus SD motif at the transposon-gene breakpoint at position 5191 of antisense ROO, although it frequently provided 5´- sequence to transposon-

254 gene chimeric RNAs. However, the sequence around position 5191 matched the consensus
255 motif, with the exception of a GT-to-GC conversion (see Figure 4 – figure supplement 1).
256 Taken together, our analysis revealed that transposons introduce many alternative splice
257 sites, which are recognised by the host cell spliceosome to combine cellular exonic
258 sequences with sections of transposon sequence.
259
260 We also identified cases of alternative splicing to different sites within the same transposon
261 insertion. Again using ROO as an example, αβCherry flies harbour a reverse orientation
262 ROO in the intron between exons 10 and 11 of the pan-neurally expressed *mustard* (*mtd*)
263 gene, which to date has only been implicated in fly innate immunity (Wang et al., 2012)
264 (Figure 5f). RNAseq revealed a complex collection of *mtd* splice variants that incorporated
265 different fragments of ROO (Figure 5g). SD sites upstream of this ROO came from the end
266 of either *mtd* exon 11. or 13. and these spliced in to the corresponding SA at position 5462
267 within ROO (Figure 5g). We also found three different SD sites (at positions 641, 2784 and
268 5191) within ROO, which spliced out to the closest downstream SA (exon 6) of *mtd*.
269 Therefore, this ROO element substantially increases the *mtd* mRNA isoform repertoire.
270 Without ROO the *mtd* locus can express 23 isoforms whereas with ROO it can generate 68
271 differentially spliced mRNAs.
272
273 We identified 147 other genes whose transcript diversity was similarly increased by
274 transposon insertions. These alternative transcripts incorporate 43 different transposon
275 families which each introduce cryptic SA and/or SD sites into host genes (see
276 Supplementary Table 5). For example, we found a sense insertion of BLOOD inside the
277 *Dscam2* gene which encodes the transmembrane Down Syndrome cell adhesion molecule
278 2. Chimeric reads indicate that transcription of *Dscam2* is frequently initiated in BLOOD,
279 which is then spliced into exon 33 (the second exon) of the gene. This splicing event
280 combines ORF2 of BLOOD with the remaining exons of *Dscam2* and correctly aligns the
281 reading frames of the two transcripts, generating a novel N-terminus (Figure 5 – figure
282 supplement 1). We also observed cases where transposon chimera resulted in exon
283 skipping (e.g. the above mentioned ROO in *mtd* and 412 inside *tequila*, Figure 5 – figure
284 supplement 2). Most transposon chimera resulted from intronic insertions, but we also
285 detected one case where a HOBO insertion resided in the exon of the *CG31705* gene. This
286 HOBO introduced a cryptic SA site which was spliced to the upstream SD from the first
287 exon, creating a truncated *CG31705* transcript (Figure 5 – figure supplement 3). Together
288 these data show that a broad range of *Drosophila* transposons are alternatively spliced into
289 mRNAs producing many more isoforms of a large number of neurally expressed genes.
290

291 **Alternative splicing into and out of transposons can be highly penetrant**
292 Chimeric transcripts could be inconsequential to a cell if they only constitute a small
293 percentage of the overall transcript repertoire of a given gene. We therefore quantified the
294 percentage of mRNAs produced from a transposon harbouring gene that include transposon
295 sequence. To do this we analysed sites where transposons were spliced into an exon-intron
296 junction of a gene. For each gene we counted the number of reads spanning transposon-
297 exon boundaries, and the number of reads that spanned the exon immediately up- and
298 downstream of the transposon insertion (Figure 6a). This analysis showed that for some
299 genes, all derived mRNAs contained transposon sequences. For example, all spliced copies
300 of the isoform B of the Allatostatin A receptor 1 (*AstA-R1*) contained a section of ROO, and
301 every transcript of *Piezo-like* (*Pzl*), a gene encoding a predicted mechanosensitive ion
302 channel, ended in the I-element instead of exon 1 (Hu et al., 2019). All mRNAs retrieved
303 from *Mec2* contained TRANSPAC as the most 5´ sequence, suggesting that transcripts
304 might initiate within the TRANSPAC transposon and spliced to the SD of *Mec2* exon 2. On
305 average, transposons contributed to 14% of transcripts derived from a specific gene (Figure
306 6b, Supplementary Table 7). Insertions in genes on the X chromosome, resulted in a higher
307 average percentage of chimeric transcripts (27% vs. 13% for the rest of the genome) and a
308 larger number of cases where 75% or more of transcripts were chimeric. Insertions on the X
309 chromosome are hemizygous in male flies and our samples were generated by pooling an
310 equal number of male and female flies. The increased chimera rate on the X might therefore
311 reflect the smaller number of different X chromosomes when compared to the rest of the
312 genome. For example, we found that the X-linked *cacophony* (*cac*) gene, which encodes a
313 voltage-gated calcium channel, harboured a sense-orientation BLASTOPIA (Smith et al.,
314 1996). This transposon insertion resulted in 54.7% of *cac* transcripts being truncated in
315 αβCherry fly samples, potentially missing the last 8-11 coding exons, suggesting that many
316 flies in this strain are likely mutant for the *cac* gene (Figure 5 – figure supplement 4). Another
317 interesting example on the X chromosome of αβCherry flies is *Beadex* (*Bx*) which encodes a
318 long-term memory relevant LIM-type transcription factor (Hirano et al., 2016). A sense
319 NOMAD insertion gives rise to at least two new *Bx* transcript isoforms (Figure 5 – figure
320 supplement 5), which constitute 9.8% of all *Bx* transcripts.
321
322 **Splicing into transposons is common and varies between strains**
323 The transposon complement is highly variable between fly strains. We therefore tested
324 whether other fly strains express chimeric gene:transposon mRNAs by analysing three
325 previously published mRNA sequencing data sets (Croset et al., 2018; Daines et al., 2011;
326 MacKay et al., 2012). Although these prior studies generated shorter paired-end RNAseq
327 reads, than those collected here, we were still able to find chimeric mRNAs in all three data

328 sets (Supplementary Table 8). Some transposon:gene chimera were conserved across all
329 strains, whilst others appeared to be strain-specific. 318 of the 887 chimera identified in our
330 αβCherry flies were present in at least one of the three other data sets, whereas 120 of
331 those occurred in at least three of the four strains. Chimera that were not detected in data
332 from other strains could either reflect genomic heterogeneity between the tested fly strains,
333 or the absence of evidence could result from lower sequencing coverage. Nevertheless,
334 these results demonstrate the prevalence of cellular mRNAs containing transposon
335 sequence.

Discussion

Somatic transposition in neurons has been proposed to contribute to age-dependent neuronal decline in wildtype and disease models of *Drosophila* and (Li, e al., 2013; Guo et al., 2018; Sun et al., 2018). Although the frequency of neural transposition is debated, expression is a prerequisite for movement. Therefore, transposons can only mobilize in cells that express full-length elements, or transposon mRNAs that encode enzymes permitting other elements to move in *trans*. It is therefore important to understand how transposon expression is controlled in the brain. Here, we combined single-cell expression data from the *Drosophila* midbrain with high-coverage gDNA sequence data of the same fly strain and find that the majority, if not all, expressed transposon sequences are parts of chimeric mRNAs with cellular genes.

Transposons residing in introns have previously been shown to contribute novel exons to several genes (Nekrutenko and Li, 2001). In addition long non-coding (lnc) RNAs frequently contain transposon sequences (Kapusta et al., 2013). We found transposon exonisation to be highly prevalent in the *Drosophila* brain. Transposons within the coding regions of genes and those in introns dramatically increase the transcript repertoire by introducing new splice variants. At this stage it is difficult to definitively determine the whole-genome functional consequences of splicing into transposons because we most often only retrieve the sequence across the splice junctions. Furthermore, although each transposon has a known consensus sequence individual copies are highly polymorphic. Nevertheless, our sequencing shows that transposon exonisation often truncates and/or changes the amino acid sequence of the encoded gene products, potentially changing protein structure and function. We did also identify several examples where the inclusion of transposon sequence conserved the reading frame of the host gene, likely generating a novel chimeric protein. Amongst the 148 transposon harbouring genes identified in this study, there are several that we have described in detail for which the observed locus disruption and altered expression would be expected to have significant consequences for neural function. Flies harbouring HOBO in *Sh* and BLASTOPIA in *cac* might exhibit altered voltage-gated currents, whereas those with ROO in *AstA-R1* will respond differently to the modulatory Allatostatin A neuropeptide. We also described insertions of 412 in *teq* and NOMAD in *Bx*, two genes which have been implicated in long-term memory formation.

Some transposons provide more splice sites than others. Our analysis of the abundant ROO retrotransposon (found in sense orientation inside 48 genes, and in antisense orientation inside 59 genes in our strain) provides a good example, and the insertion in *mtd* exemplifies the extended variance transposons can introduce to cellular transcription units. Interestingly,

373 antisense insertions of ROO provide more potential SA and SD sites than sense orientation
374 ROO. Insertions of ROO that are sense to the expression of the host gene were found to be
375 mainly part of pre-mRNA, from which functional reverse transcriptase could potentially be
376 translated. In contrast, antisense ROO introduces over 10 times more cryptic splice sites
377 (compare Figure 5b and c).
378
379 mRNA molecules that contain transposon sequences might be susceptible to short-
380 nucleotide mediated gene-silencing (Malone and Hannon, 2009), as recently reported for
381 LINE-2 containing mRNAs and LINE-2 derived microRNAs in humans (Petri et al., 2019).
382 This would provide a challenge for the cells expressing transposon-targeting piRNAs in
383 differentiating between chimeric transcripts and full-length transposon sequences. It is worth
384 noting that transposon-directed piRNAs have been identified in the fly brain. It is therefore
385 conceivable that transposon sequence permits cellular mRNAs to be selectively regulated.
386 In addition, transposon sequence might confer the capacity to be specifically trafficked within
387 the cell, and even between cells (Ashley et al., 2018; Pastuzyn et al., 2018).
388
389 The process of transposable elements acquiring new cellular functions that benefit the host
390 cell is called transposon exaptation (Gould and Vrba, 2013). Several examples of exaptation
391 events during the evolution of eukaryotes have been reported. How these functional
392 transitions occur is, however, not fully understood (Joly-Lopez and Bureau, 2018). Stress-
393 induced transposon mobilisation has been observed in many species, and it has been
394 hypothesized that these mobilisation events trigger the formation of new transposon-gene
395 chimera. Our results reveal a new mechanism by which transposons participate in the
396 generation of new gene variants. We show that transposons do not need to mobilise in order
397 to form chimeric mRNA molecules. Instead, the cellular gene spicing machinery frequently
398 uses intronic transposon insertions to increase transcriptional diversity.
399
400 Transposon sequences in the gDNA can deliver enhancer elements to cellular genes and
401 thereby influence their expression. However, our results do not support the idea that
402 transposons provide enhancer sequences contributing to neural expression of neighbouring
403 genes. If this was the case, we would expect to have found that cellular genes that harbour
404 the same type of transposon are more likely to be expressed in the same cells. Our data
405 instead show that transposon expression is dictated by the genes they are inserted within.
406 This is further supported by the fact that many genes that share transposon insertions with
407 neurally expressed genes were not expressed in the brain.
408

Our studies also introduce important practical concerns for the analysis of transposon expression in somatic tissue and disease models. Several previous studies have used Quantitative PCR (qPCR) to measure levels of transposon expression in mutant flies and disease models. Since qPCR probes are usually not designed to cross transposon-gene breakpoints, they cannot distinguish autonomous transposon expression from chimeric mRNA. Similarly, standard RNA sequencing protocols rely on the alignment of cDNA fragments to the reference genome and would not identify chimeric reads as non-autonomous transposon expression. Baseline and changing cell-specific expression of host genes that form chimeric transcripts with transposons can therefore be misinterpreted as cell-restricted autonomous transposon expression and mobilization.

Our data also constrain somatic transposition. If all transposon expression depends on the neighbouring host gene, only cells expressing that host gene can be susceptible to transposition of that element. This would mean that GYPSY could only be active in glia, if the fly strains being studied harbour a copy of GYPSY in a glial-expressed gene. Interestingly, although we found sense GYPSY sequences in mRNAs for 14 different genes, we did not detect glial GYPSY expression in our αβCherry flies.

Analysis of RNA-seq data from other fly strains suggests that more than half of the chimeric transposon transcripts we identified in αβCherry flies are unique to this strain. This finding alone demonstrates the incredible heterogeneity of the transposon complement between strains. In addition, our prior genome sequencing revealed large differences between individual αβCherry flies. Given the broad range of target genes that we have identified to form chimeric mRNA with transposable elements, it will be important to understand the functional consequences of fixed and variable transposons inside genes for the host organism. Nevertheless, it seems highly likely that polymorphism of transposon load and the distribution of transposons across the host genome could contribute towards heterogeneity of neural function, and neurological pathology, between individual animals.

Methods

Fly strains

All experiments were performed on αβCherry flies, which were generated by crossing MB008b females (Aso et al., 2014) with w-; +; UAS-mCherry males. Flies were raised on standard molasses at 25°C, 40-50% humidity and 12 hr:12 hr dark-light cycles.

Long-read mRNA sequencing

For RNA extraction, groups of ~50 flies were frozen in liquid nitrogen and vortexed for 6 x 30 sec to separate heads from abdomens. Heads were isolated using a sieve. To avoid gDNA contamination, mRNA was purified with a combination of protocols. Samples were first processed with a column-based kit (RNeasy Mini kit, Qiagen, UK), including the optional on-column DNAseI digestion. Next, mRNA was extracted from total RNA using oligo-dT magnetic beads (NEB, Ipswich, MA) and the mRNA was purified again using the RNA columns. Finally, sequencing libraries were generated using oligo-dT magnetic beads from a strand-specific mRNA library preparation kit (TruSeq, Illumina, San Diego, CA), with 17 cycles of PCR amplification. Fragmentation was optimized to obtain ~350nt long fragments. Whole-genome sequencing was performed on a HiSeq 2500, with 250nt paired-end reads. We mapped the long reads using MRTemp, as previously described(Treiber and Waddell, 2017).

Single-cell read alignments

The Drosophila melanogaster reference genome release 6.25 was used for all sequence alignments. Transposon reference sequences were taken from Repbase (Jurka, 2000; Kaminker et al., 2002). Repetitive sequences in the *Drosophila* reference genome were masked using Repeatmasker (Smit et al.). Single-cell sequencing data was processed with a custom-built data processing pipeline, which is available on GitHub. The masked reference genome, as well as a gene reference file (refFlat) with all genes and each unique reference transposon sequence is provided as supplementary data.

Single-cell data analysis

Digital Gene Expression (DGE) matrices were generated as previously described (Butler et al., 2018). Rscripts can be downloaded as a supplementary file. In summary, DGE's were filtered (≥ 800 UMIs, ≥ 400 features) and 8 replicates were merged. Gene and transposon expressions levels were normalised separately. Marker genes were taken from Croset et al. (2018).

476 **Co-expression analysis**

477 Co-expression was quantified by calculating the Co-expression Disequilibrium (CD, see
478 main text). The R-code snippet is available through Github. For the statistical analysis, a
479 non-parametric test was performed. CD values between every gene- and transposon
480 combination were ranked within each biological replicate, p-values were calculated using the
481 student t-test and corrected for multiple comparisons using the Benjamini-Hochberg
482 correction. In addition, CD values were calculated for every tested transposon with a set of
483 10 randomly assigned genes (or transposons).

484

485 **Mapping germline transposon insertions in the fly**

486 Germline transposon insertions were mapped with single-nucleotide resolution using
487 previously published gDNA data from the αβCherry fly strain and MRTemp (Treiber and
488 Waddell, 2017). A new, purpose-built, multi-functional sequence analysis pipeline called
489 TEchim was developed. TEchim has 5 key functions: 1. generation of support files, including
490 a masked reference genome and endogenous intron-exon junctions. (input files: reference
491 genome, list of genes, list of transposon sequences). 2. alignment of un-stranded genomic
492 DNA sequence data of multiple sequencing lanes and multiple biological replicates,
493 detection of chimeric sequence fragments with single-nucleotide resolution, and the
494 generation of summary output tables. 3. alignment of stranded cDNA data, detection of
495 chimeric fragments, quantification of reads 4. generation of matching immobile genetic
496 elements (IGE, see main text), analysis of these IGEs. These data are then used to
497 determine sample-specific detection thresholds. 5. Quantification of LTR-gene and LTR-
498 transposon reads (see Figure 4). Detailed descriptions and manuals are available on Github.

499

500 **Splice acceptor (SA) and donor (SD) motif analysis**

501 SA and SD motifs in the *Drosophila melanogaster* reference genome were generated by
502 randomly selecting 500 known SA and SD sites from exons and screening for motifs in these
503 sequences using the MEME suite (Bailey and Elkan, 1994) (Figure 4 – figure supplement 1).
504 These motifs were then searched in sequence sections across transposon-gene breakpoints
505 using FIMO (Grant et al., 2011).

506 **References**

507

508 Ashley, J., Cordy, B., Lucia, D., Fradkin, L.G., Budnik, V., and Thomson, T. (2018).
509 Retrovirus-like Gag Protein Arc1 Binds RNA and Traffics across Synaptic Boutons. Cell *172*,
510 262-274.e11.
511 Aso, Y., Hattori, D., Yu, Y., Johnston, R.M., Iyer, N.A., Ngo, T.T.B., Dionne, H., Abbott, L.F.,
512 Axel, R., Tanimoto, H., et al. (2014). The neuronal architecture of the mushroom body
513 provides a logic for associative learning. Elife *3*, e04577.
514 Bailey, T.L., and Elkan, C. (1994). Fitting a mixture model by expectation maximization to
515 discover motifs in biopolymers. Proceedings. Int. Conf. Intell. Syst. Mol. Biol. *2*, 28–36.
516 Baillie, J.K., Barnett, M.W., Upton, K.R., Gerhardt, D.J., Richmond, T.A., De Sapio, F.,
517 Brennan, P., Rizzu, P., Smith, S., Fell, M., et al. (2011). Somatic retrotransposition alters the
518 genetic landscape of the human brain. Nature *479*, 534–537.
519 Britten, R.J., and Kohne, D.E. (1968). Repeated sequences in DNA. Hundreds of thousands
520 of copies of DNA sequences have been incorporated into the genomes of higher organisms.
521 Science *161*, 529–540.
522 Butler, A., Hoffman, P., Smibert, P., Papalexi, E., and Satija, R. (2018). Integrating single-
523 cell transcriptomic data across different conditions, technologies, and species. Nat.
524 Biotechnol. *36*, 411–420.
525 Chung, N., Jonaid, G.M., Quinton, S., Ross, A., Sexton, C.E., Alberto, A., Clymer, C.,
526 Churchill, D., Navarro Leija, O., and Han, M. V. (2019). Transcriptome analyses of tumor-
527 adjacent somatic tissues reveal genes co-expressed with transposable elements. Mob. DNA
528 *10*, 1–22.
529 Coufal, N.G., Garcia-Perez, J.L., Peng, G.E., Yeo, G.W., Mu, Y., Lovci, M.T., Morell, M.,
530 O'Shea, K.S., Moran, J. V., and Gage, F.H. (2009). L1 retrotransposition in human neural
531 progenitor cells. Nature *460*, 1127–1131.
532 Croset, V., Treiber, C.D., and Waddell, S. (2018). Cellular diversity in the Drosophila
533 midbrain revealed by single-cell transcriptomics. Elife *7*.
534 Daines, B., Wang, H., Wang, L., Li, Y., Han, Y., Emmert, D., Gelbart, W., Wang, X., Li, W.,
535 Gibbs, R., et al. (2011). The Drosophila melanogaster transcriptome by paired-end RNA
536 sequencing. Genome Res. *21*, 315–324.
537 Evrony, G.D., Cai, X., Lee, E., Hills, L.B., Elhosary, P.C., Lehmann, H.S., Parker, J.J.,
538 Atabay, K.D., Gilmore, E.C., Poduri, A., et al. (2012). Single-neuron sequencing analysis of
539 l1 retrotransposition and somatic mutation in the human brain. Cell *151*, 483–496.
540 Evrony, G.D., Lee, E., Park, P.J., and Walsh, C.A. (2016). Resolving rates of mutation in the
541 brain using single-neuron genomics. Elife *5*, 1–32.
542 Faulkner, G.J., Kimura, Y., Daub, C.O., Wani, S., Plessy, C., Irvine, K.M., Schroder, K.,

543 Cloonan, N., Steptoe, A.L., Lassmann, T., et al. (2009). The regulated retrotransposon
544 transcriptome of mammalian cells. Nat. Genet. *41*, 563–571.
545 Gould, S.J., and Vrba, E.S. (2013). Exaptation-A Missing Term in the Science of Form
546 Exaptation-a missing term in the science of form. Paleobiology *8*, 4–15.
547 Grant, C.E., Bailey, T.L., and Noble, W.S. (2011). FIMO: Scanning for occurrences of a
548 given motif. Bioinformatics *27*, 1017–1018.
549 Guo, C., Jeong, H.H., Hsieh, Y.C., Klein, H.U., Bennett, D.A., De Jager, P.L., Liu, Z., and
550 Shulman, J.M. (2018). Tau Activates Transposable Elements in Alzheimer's Disease. Cell
551 Rep. *23*, 2874–2880.
552 Hirano, Y., Ihara, K., Masuda, T., Yamamoto, T., Iwata, I., Takahashi, A., Awata, H.,
553 Nakamura, N., Takakura, M., Suzuki, Y., et al. (2016). Shifting transcriptional machinery is
554 required for long-term memory maintenance and modification in Drosophila mushroom
555 bodies. Nat. Commun. *7*, 1–14.
556 Hu, Y., Wang, Z., Liu, T., and Zhang, W. (2019). Piezo-like Gene Regulates Locomotion in
557 Drosophila Larvae. Cell Rep. *26*, 1369-1377.e4.
558 International Human Genome Sequencing Consortium, Eric S. Lander, Lauren M. Linton,
559 Bruce Birren, Chad Nusbaum, Michael C. Zody, Jennifer Baldwin, Keri Devon, Ken Dewar,
560 and Michael Doyle (2001). Initial sequencing and analysis of the human genome. Nature
561 *409*, 860–921.
562 Izquierdo, M. (1994). Ubiquitin genes and ubiquitin protein location in polytene
563 chromosomes of Drosophila. Chromosoma *103*, 193–197.
564 Joly-Lopez, Z., and Bureau, T.E. (2018). Exaptation of transposable element coding
565 sequences. Curr. Opin. Genet. Dev. *49*, 34–42.
566 Jurka, J. (2000). Repbase Update: A database and an electronic journal of repetitive
567 elements. Trends Genet. *16*, 418–420.
568 Kaminker, J.S., Bergman, C.M., Kronmiller, B., Carlson, J., Svirskas, R., Patel, S., Frise, E.,
569 Wheeler, D.A., Lewis, S.E., Rubin, G.M., et al. (2002). The transposable elements of the
570 Drosophila melanogaster euchromatin: a genomics perspective. Genome Biol *3*.
571 Kaplan, W.D., and Trout, W.E. (1969). The behavior of four neurological mutants of
572 Drosophila. Genetics *61*, 399–409.
573 Kapusta, A., Kronenberg, Z., Lynch, V.J., Zhuo, X., Ramsay, L.A., Bourque, G., Yandell, M.,
574 and Feschotte, C. (2013). Transposable Elements Are Major Contributors to the Origin,
575 Diversification, and Regulation of Vertebrate Long Noncoding RNAs. PLoS Genet. *9*.
576 Kazazian, H.H. (2011). Mobile DNA transposition in somatic cells. BMC Biol. *9*, 2–5.
577 Ketchum, K., Ketchum, K., Hoskins, R., Hoskins, R., Wang, X., Wang, X., Smith, T., Smith,
578 T., Gocayne, J., Gocayne, J., et al. (2000). The genome sequence of Drosophila
579 melanogaster. Science (80-.). *287*, 2185–2195.

580 Krug, L., Chatterjee, N., Borges-Monroy, R., Hearn, S., Liao, W.W., Morrill, K., Prazak, L.,
581 Rozhkov, N., Theodorou, D., Hammell, M., et al. (2017). Retrotransposon activation
582 contributes to neurodegeneration in a Drosophila TDP-43 model of ALS.
583 Lavie, L., Maldener, E., Brouha, B., Meese, E.U., and Mayer, J. (2004). The human L1
584 promoter: Variable transcription initiation sites and a major impact of upstream flanking
585 sequence on promoter activity. Genome Res. *14*, 2253–2260.
586 Lewontin, R.C., and Kojima, K. (1960). The Evolutionary Dynamics of Complex
587 Polymorphisms. Evolution (N. Y). *14*, 458–472.
588 Li, W., Prazak, L., Chatterjee N., Grüninger, S., Krug, L., Theodorou, D., Dubnau, J. (2013).
589 Activation of transposable elements during aging and neuronal decline in Drosophila.
590 Neurosci. Nat. *16*, 529–531.
591 Li, W., Jin, Y., Prazak, L., Hammell, M., and Dubnau, J. (2012). Transposable Elements in
592 TDP-43-Mediated Neurodegenerative Disorders. PLoS One *7*, 1–10.
593 MacKay, T.F.C., Richards, S., Stone, E.A., Barbadilla, A., Ayroles, J.F., Zhu, D., Casillas, S.,
594 Han, Y., Magwire, M.M., Cridland, J.M., et al. (2012). The Drosophila melanogaster Genetic
595 Reference Panel. Nature *482*, 173–178.
596 Macosko, E.Z., Basu, A., Satija, R., Nemesh, J., Shekhar, K., Goldman, M., Tirosh, I.,
597 Bialas, A.R., Kamitaki, N., Martersteck, E.M., et al. (2015). Highly parallel genome-wide
598 expression profiling of individual cells using nanoliter droplets. Cell *161*, 1202–1214.
599 Malone, C.D., and Hannon, G.J. (2009). Small RNAs as Guardians of the Genome. Cell *136*,
600 656–668.
601 Muotri, A.R., Chu, V.T., Marchetto, M.C.N., Deng, W., Moran, J. V., and Gage, F.H. (2005).
602 Somatic mosaicism in neuronal precursor cells mediated by L1 retrotransposition. Nature
603 *435*, 903–910.
604 Nekrutenko, A., and Li, W.H. (2001). Transposable elements are found in a large number of
605 human protein-coding genes. Trends Genet. *17*, 619–621.
606 Pastuzyn, E.D., Day, C.E., Kearns, R.B., Kyrke-Smith, M., Taibi, A. V., McCormick, J.,
607 Yoder, N., Belnap, D.M., Erlendsson, S., Morado, D.R., et al. (2018). The Neuronal Gene
608 Arc Encodes a Repurposed Retrotransposon Gag Protein that Mediates Intercellular RNA
609 Transfer. Cell *172*, 275-288.e18.
610 Perrat, P.N., Dasgupta, S., Wang, J., Theurkauf, W., Weng, Z., Rosbash, M., and Waddell,
611 S. (2013). Heterogeneity in the Drosophila Brain. *340*, 91–96.
612 Petri, R., Brattås, P.L., Sharma, Y., Jönsson, M.E., Pircs, K., Bengzon, J., and Jakobsson, J.
613 (2019). LINE-2 transposable elements are a source of functional human microRNAs and
614 target sites. PLOS Genet. *15*, e1008036.
615 Philippe, C., Vargas-Landin, D.B., Doucet, A.J., Van Essen, D., Vera-Otarola, J., Kuciak, M.,
616 Corbin, A., Nigumann, P., and Cristofari, G. (2016). Activation of individual L1

617 retrotransposon instances is restricted to cell-type dependent permissive loci. Elife *5*, 1–30.
618 Rangwala, S.H., Zhang, L., and Kazazian, H.H. (2009). Many LINE1 elements contribute to
619 the transcriptome of human somatic cells. Genome Biol. *10*, 1–18.
620 Roebroek, A.J.M., Pauli, I.G.L., Zhang, Y., and van de Ven, W.J.M. (1991). cDNA sequence
621 of a Drosophila melanogaster gene, Dfur1, encoding a protein structurally related to the
622 subtilisin-like proprotein processing enzyme furin. FEBS Lett. *289*, 133–137.
623 Smit, A.F.A., Hubley, R., and Green, P. RepeatMasker.
624 Smith, L.A., Wang, X.J., Peixoto, A.A., Neumann, E.K., Hall, L.M., and Hall, J.C. (1996). A
625 Drosophila calcium channel α1 subunit gene maps to a genetic locus associated with
626 behavioral and visual defects. J. Neurosci. *16*, 7868–7879.
627 Stephens, R.M., and Schneider, T.D. (1992). Features of spliceosome evolution and function
628 inferred from an analysis of the information at human splice sites. J. Mol. Biol. *228*, 1124–
629 1136.
630 Sun, W., Samimi, H., Gamez, M., Zare, H., and Frost, B. (2018). Pathogenic tau-induced
631 piRNA depletion promotes neuronal death through transposable element dysregulation in
632 neurodegenerative tauopathies. Nat. Neurosci. *21*, 1038–1048.
633 Treiber, C.D., and Waddell, S. (2017). Resolving the prevalence of somatic transposition in
634 drosophila. Elife *6*.
635 Upton, K.R., Gerhardt, D.J., Jesuadian, J.S., Richardson, S.R., Sánchez-Luque, F.J.,
636 Bodea, G.O., Ewing, A.D., Salvador-Palomeque, C., Van Der Knaap, M.S., Brennan, P.M.,
637 et al. (2015). Ubiquitous L1 mosaicism in hippocampal neurons. Cell *161*, 228–239.
638 Wan, H.I., DiAntonio, A., Fetter, R.D., Bergstrom, K., Strauss, R., and Goodman, C.S.
639 (2000). Highwire regulates synaptic growth in Drosophila. Neuron *26*, 313–329.
640 Wang, Z., Berkey, C.D., and Watnick, P.I. (2012). The Drosophila Protein Mustard Tailors
641 the Innate Immune Response Activated by the Immune Deficiency Pathway. J. Immunol.
642 *188*, 3993–4000.
643 Zhang, W., Wu, J., Ward, M.D., Yang, S., Chuang, Y.A., Xiao, M., Li, R., Leahy, D.J., and
644 Worley, P.F. (2015). Structural basis of arc binding to synaptic proteins: Implications for
645 cognitive disease. Neuron *86*, 490–500.
646

Author Contributions

C.D.T. and S.W. conceived the project and wrote the manuscript. C.D.T. performed and analysed all experiments.

Statement of competing interests

Both authors declare no financial and non-financial competing interests.

653 **Figure Legends**

654

655 **Figure 1. Single-cell transcriptomics reveals patterned transposon expression in the**
656 ***Drosophila* midbrain.**

657 **A** Two-dimensional reduction (tSNE) of 14,804 *Drosophila* midbrain cells, based on gene
658 expression levels. Colours represent cell clusters (at SNN resolution of 3.5). **B-F** Mean
659 expression of transposons and neighbouring cellular genes in the relevant cell groups in 8
660 biological replicates and tSNE representation of cell-type restricted expression. **B** COPIA
661 and *twin-of-eyeless* (*toy*) in all Kenyon Cell (KC) classes. **C** NOMAD and *mushroom-body*
662 *expressed* (*mub*) in α´β´ KCs. **D** MICROPIA and *Rhodopsin 7* (*Rh7*) in the ellipsoid body **E**
663 **and F** BLOOD and *CG32521*, and 412 and *tequila* (*teq*) in glia. Values represent the mean
664 normalised number of unique molecular identifiers (UMI's) in an average cell from each cell
665 type, and from the rest of the midbrain. Error bar indicates standard error of mean (SEM).
666 Note that transposon- and gene levels were normalised separately. Blue schematic shows
667 location of cell cluster (pink) in tSNE plot. **G** Two-dimensional reduction of 14,804 *Drosophila*
668 midbrain cells, based exclusively on transposon expression levels. Colours represent cell
669 clusters (at SNN resolution of 3.5). **H and I** Mean expression of STALKER2 and *Hsp70Bc*
670 and DOC and *Furin 1* (*Fur1*) in their relevant transposon clusters and the position of the
671 cluster in the overall transposon-based tSNE (indicated in pink).

672

673 **Figure 1 – figure supplement 1. Sense strand transposon transcripts are twice as**
674 **abundant as antisense strand transcripts in the *Drosophila* midbrain.**

675 Graph showing mean expression levels across the entire midbrain of all sense and
676 antisense transposon sequences. Each data point (cross) represents one biological
677 replicate.

678

679 **Figure 1 – figure supplement 2. Transposon expression patterns are stereotyped**
680 **across biological replicates.**

681 tSNE based on transposon expression levels showing all 8 biological replicates. Each
682 replicate contributes cells to each cluster.

683

684 **Figure 2. Transposons are co-expressed with neighbouring genes.**

685 **A** Schematic and formulae describing the calculation of Co-expression Disequilibrium
686 values. **B** Examples of transposon-gene pairs that are neighbouring in the genome and co-
687 expressed across the midbrain. Pink bar represents the total transposon expression.
688 Examples are selected from the most highly expressing transposons. See Supplementary
689 Table 2 for entire list of correlated transposon-gene pairs. **C** Graph illustrating that more

690 neighbouring genes are correlated with their resident transposons than if transposons are
691 randomly assigned to genes.
692
693 **Figure 3. Chimeric transposon-gene mRNA is abundant in the midbrain.**
694 **A** Schematic of the structure of chimeric mRNA molecules, and illustrating the data
695 representation in **B**. **B** Examples of transposon-gene pairs that form chimeric mRNA. The
696 blue box contains the gene name, the section of the gene that forms a chimera and the
697 breakpoint, which is always the endogenous exon-intron junction. The red box contains the
698 transposon name, and the breakpoint(s) on the transposon. Note that for consistency,
699 transposon breakpoints are always taken from the sense orientation, starting from the core
700 transposon sequence, unless specifically indicated as [LTR]. Examples shown here are the
701 same transposon-gene pairs as in Figure 2b. For the entire list of chimera, see
702 Supplementary Table 5. **C** Graph showing the number of chimeric reads, and the combined
703 expression levels of each transposon-gene pair (pink), as well as for all 10 sets of IGE-gene
704 pairs (grey). Combined expression levels are the square root of the product of reads in both
705 transcripts of a transposon/IGE-gene pair. IGEs were used to calculate a threshold for a
706 False Discovery Rate that is less than 0.1%.
707
708 **Figure 4. LTR retrotransposon expression is predominantly non-autonomously**
709 **A** Illustration showing method of calculating the percentage of chimeric transcripts vs.
710 autonomously expressed transposon transcripts. Non-autonomous expression should result
711 in an approximate value of 0.5 for reads spanning the LTR section of transposons and the
712 intron of a neighbouring gene over the number of reads spanning the LTR and the core
713 section of the transposon. In contrast, autonomous expression would not result in LTR-gene
714 spanning reads. **B** List of all LTR transposons analysed in our mRNA data. We identified
715 LTR-gene spanning reads for every LTR transposon that is expressed in the midbrain. Error
716 bars represent standard deviation. Values have been capped at 0.5 in this graph. However,
717 some transposons produced a much higher number of LTR-gene reads (see Supplementary
718 Table 4).
719
720 **Figure 4 – figure supplement 1. Splice acceptor and donor motifs.**
721 **A** Splice acceptor motif, taken from 500 randomly chosen exon-intron junctions of
722 *Drosophila* genes. **B** splice donor motif.
723
724 **Figure 5. Transposons introduce splice sites at conserved locations.**
725 **A** Illustration of the labelling scheme in panels **B-E**. The pink bar represents the transposon;
726 light pink ends indicate the LTRs and the dark pink the core sequence. The positions of the

727 dots above the bar represent the site on the transposon where an upstream exon splice
728 donor site has merged. Every dot represents a different gene. Black lines in the top half of
729 the pink bar represent splice acceptor (SA) motifs in the transposon. Dots below the pink bar
730 indicate the location of breakpoints on the transposon that are spliced to upstream exonic
731 SA sites of different genes. Bars in the lower half indicate splice donor (SD) motifs. **B-E**
732 Representations of sense- and antisense ROO and BLOOD (to scale), with all breakpoints
733 to SA and SD sites of neighbouring genes. Note that the frequently used site on antisense
734 ROO at position 5191 is a non-consensus SD site, which lacks the expected GT motif at the
735 immediate breakpoint. The sequence around 5191 resembles the consensus SD motif,
736 although the GT is a GC. Compare TTTGGCAAGTT to motif in Figure 4 – figure supplement
737 1a. **F** Illustration of antisense ROO insertion in the *mustard* (*mtd*) gene. Only one isoform of
738 *mtd* is shown. Yellow box represents the 5´UTR, blue boxes are exons, orange box the
739 3´UTR, pink represents ROO transposon with white arrows indicating the LTRs. Breakpoint-
740 spanning gDNA reads reveal Target Site Duplication (TSD, inset). **G** Schematic of original
741 *mtd* transcript, and of three new splice isoforms.
742
743 **Figure 5 – figure supplement 1. Sense BLOOD insertion in *Dscam2*.**
744 Schematics of DScam2 mRNAs produced from locus containing BLOOD. Top shows the
745 nascent transcript spliced around the intronic full-length sense BLOOD insertion. Bottom
746 illustrates a new mRNA splice isoform, which reads through in frame from the ORF2
747 sequence of BLOOD into exon 2 of *DScam2*. The breakpoint in BLOOD is a consensus SD
748 motif. 23.2% of all *Dscam2* transcripts in fly heads are chimeric with BLOOD.
749
750 **Figure 5 – figure supplement 2. Sense 412 insertion in *tequila*.**
751 Schematics of *teq* mRNAs produced from locus containing full-length sense orientation 412
752 insertion. Top, original transcripts of *teq* splicing around 412. Bottom, and new *teq* splice
753 isoforms that include 412 sequence. 83.9% of *teq* transcripts contain 412 transposon
754 sequence. In addition, 22.4 % of 412 containing mRNAs skip exon 5 of *teq*. In 0.5% of cases
755 exons 2-5 are skipped.
756
757 **Figure 5 – figure supplement 3. Antisense HOBO insertion in *CG31705*.**
758 Schematic of *CG31705* mRNAs produced from locus containing exonic antisense HOBO
759 insertion. Transcripts containing unspliced HOBO and two additional new splice isoforms
760 that are generated by alternative splicing into HOBO are shown.
761
762 **Figure 5 – figure supplement 4. Sense BLASTOPIA insertion in *cacophony*.**

763 Schematic *cac* transcripts produced from locus containing a full-length intronic sense
764 BLASTOPIA insertion. A regular cac transcript is produced by splicing around the
765 BLASTOPIA insertion and a new truncated *cac* isoform results from splicing into
766 BLAsTOPIA. The *cac* gene is on the X chromosome, and 54.7% of *cac* transcripts in the fly
767 head are truncated by splicing into BLASTOPIA.
768
769 **Figure 5 – figure supplement 5. Sense NOMAD insertion in *Bx*.**
770 Schematic showing mRNAs produced from locus containing sense intronic NOMAD
771 insertion. Original transcript of *Bx* is generated by splicing around NOMAD. New splice
772 isoforms contain fragments of NOMAD. 9.8% of transcripts that start with the *Bx* 5´UTR are
773 spliced into NOMAD.
774
775 **Figure 6. High penetrance of transposon-containing splice isoforms.**
776 **A** Schematic showing method used to calculate the frequency of transposon chimera
777 produced from a given gene. The number of reads that span the exon-transposon junction
778 were divided by the total number of reads that map beyond the exon-intron junction (exon-
779 transposon reads plus reads that partially map to the exon immediately downstream of the
780 transposon insertion. **B** Examples of chimeric transposon-gene transcripts detected in fly
781 heads. Many genes are almost exclusively expressed as chimeric transcripts with
782 transposon sequence. See Supplementary Table 7 for complete list.

Figure 1

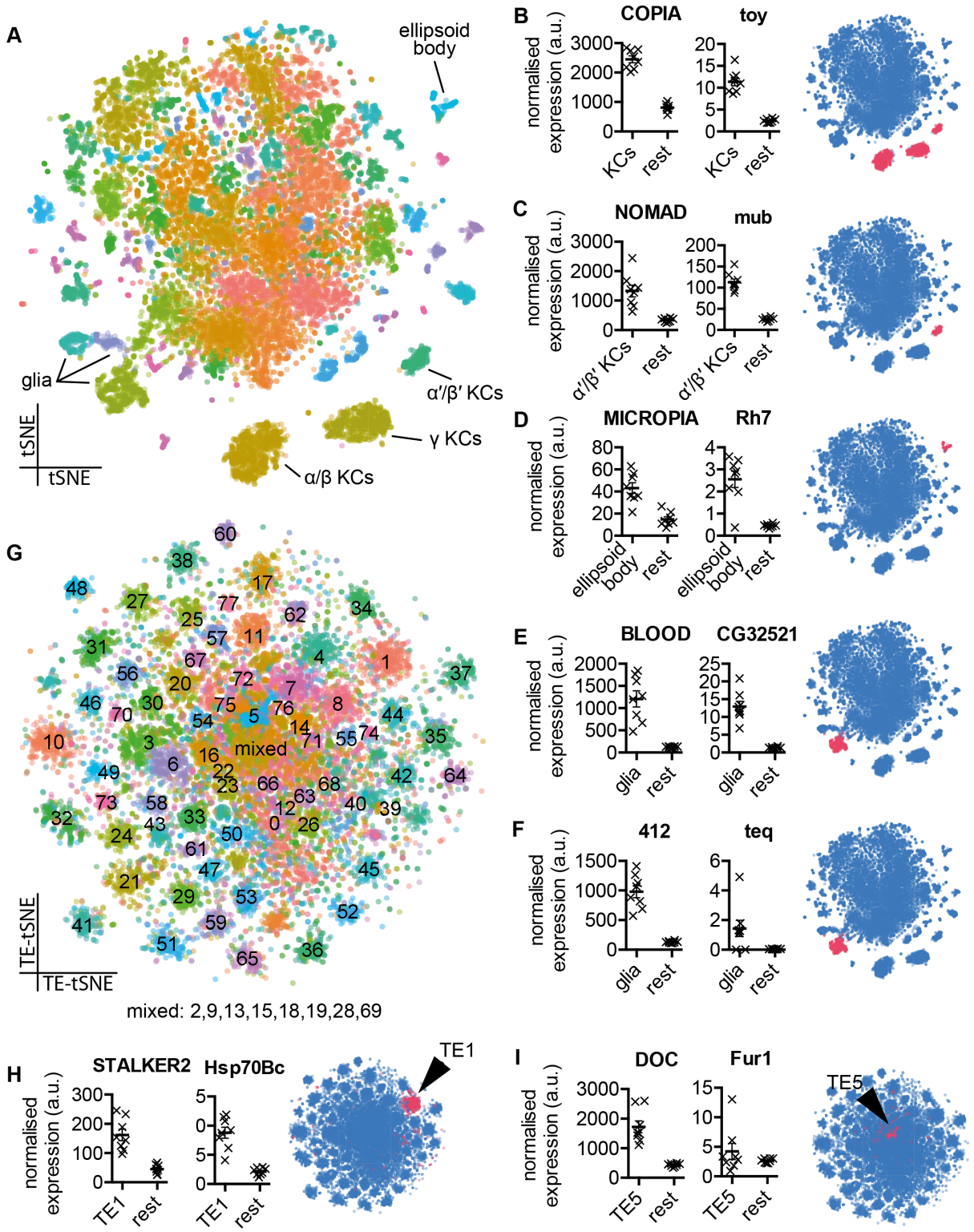

783

784

Figure 1 - Figure supplement 1

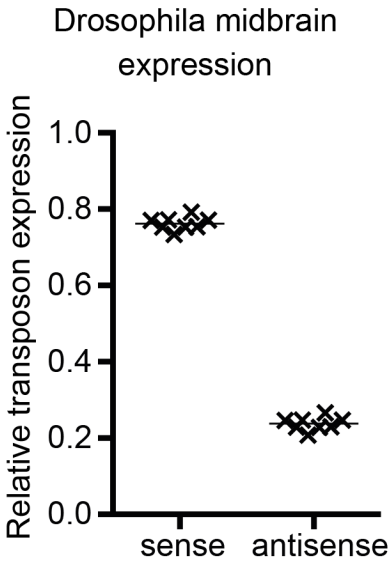

785

786

Figure 1 - figure supplement 2

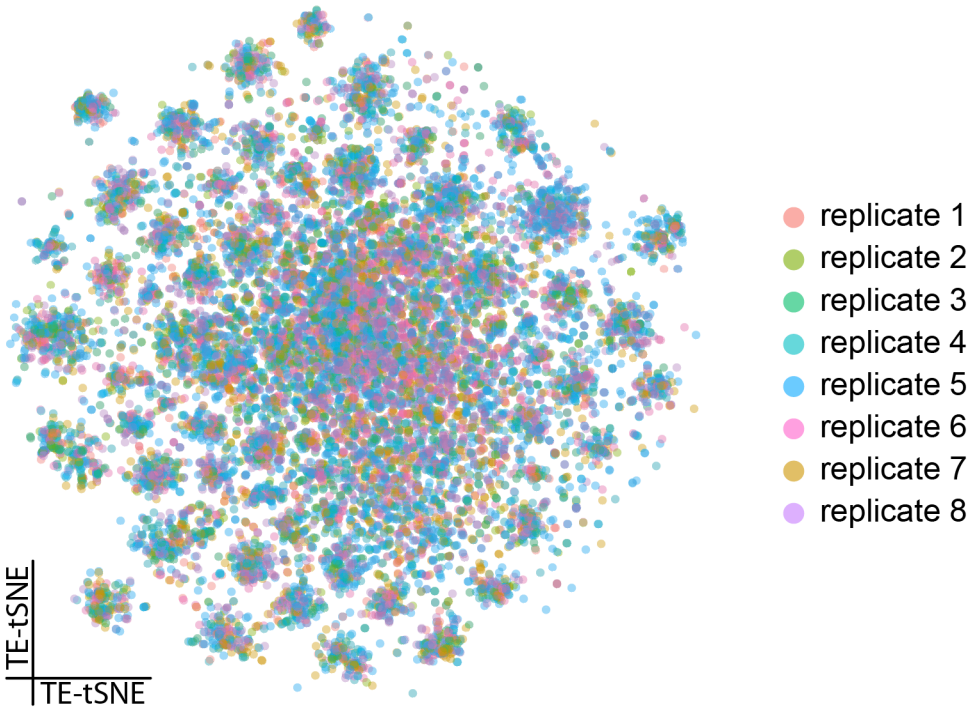

Figure 2

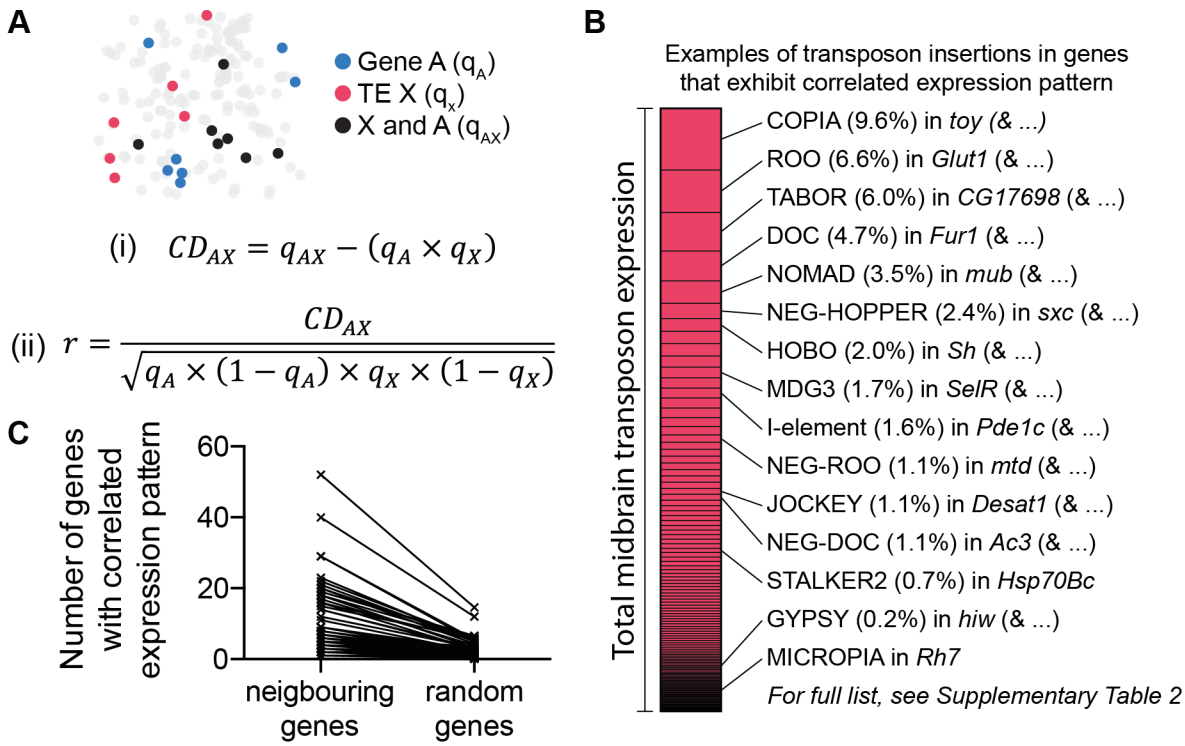
A
Gene A (q_A)
TE X (q_x)
X and A (q_{AX})
(i) $CD_{AX} = q_{AX} - (q_A \times q_X)$
(ii) $r = \frac{CD_{AX}}{\sqrt{q_A \times (1 - q_A) \times q_X \times (1 - q_X)}}$
B
Examples of transposon insertions in genes that exhibit correlated expression pattern
Total midbrain transposon expression
COPIA (9.6%) in *toy (& ...)*
ROO (6.6%) in *Glut1* (& ...)
TABOR (6.0%) in *CG17698* (& ...)
DOC (4.7%) in *Fur1* (& ...)
NOMAD (3.5%) in *mub* (& ...)
NEG-HOPPER (2.4%) in *sxc* (& ...)
HOBO (2.0%) in *Sh* (& ...)
MDG3 (1.7%) in *SelR* (& ...)
I-element (1.6%) in *Pde1c* (& ...)
NEG-ROO (1.1%) in *mtd* (& ...)
JOCKEY (1.1%) in *Desat1* (& ...)
NEG-DOC (1.1%) in *Ac3* (& ...)
STALKER2 (0.7%) in *Hsp70Bc*
GYPSY (0.2%) in *hiw* (& ...)
MICROPIA in *Rh7*
For full list, see Supplementary Table 2
C
Number of genes with correlated expression pattern
60
40
20
0
neigbouring genes
random genes

Figure 3

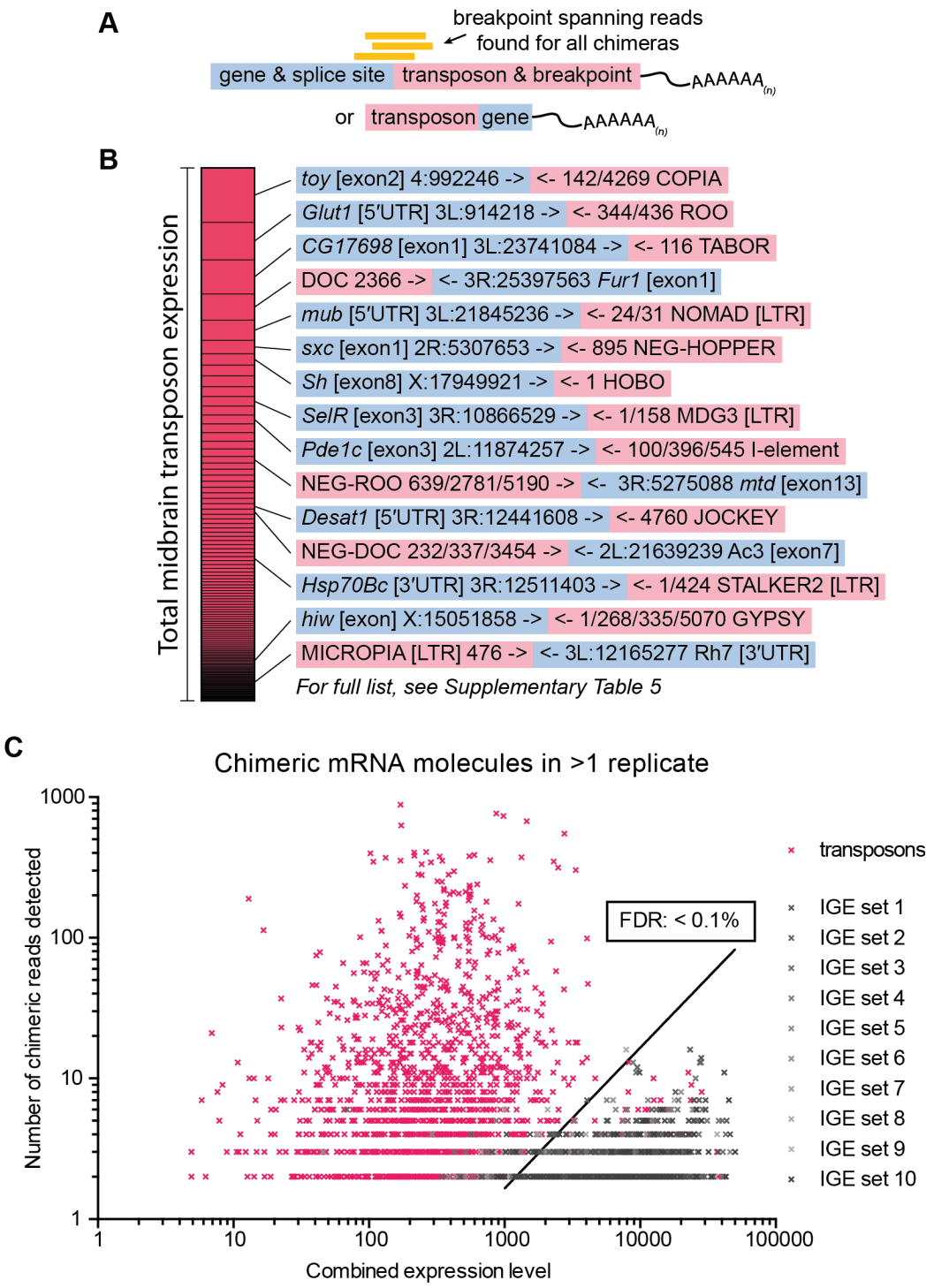
A
breakpoint spanning reads
found for all chimeras
gene & splice site
transposon & breakpoint
AAAAAA(n)
or
transposon
gene
AAAAAA(n)
B
Total midbrain transposon expression
toy [exon2] 4:992246 -> <- 142/4269 COPIA
Glut1 [5'UTR] 3L:914218 -> <- 344/436 ROO
CG17698 [exon1] 3L:23741084 -> <- 116 TABOR
DOC 2366 -> <- 3R:25397563 Fur1 [exon1]
mub [5'UTR] 3L:21845236 -> <- 24/31 NOMAD [LTR]
sxc [exon1] 2R:5307653 -> <- 895 NEG-HOPPER
Sh [exon8] X:17949921 -> <- 1 HOBO
SelR [exon3] 3R:10866529 -> <- 1/158 MDG3 [LTR]
Pde1c [exon3] 2L:11874257 -> <- 100/396/545 I-element
NEG-ROO 639/2781/5190 -> <- 3R:5275088 mtd [exon13]
Desat1 [5'UTR] 3R:12441608 -> <- 4760 JOCKEY
NEG-DOC 232/337/3454 -> <- 2L:21639239 Ac3 [exon7]
Hsp70Bc [3'UTR] 3R:12511403 -> <- 1/424 STALKER2 [LTR]
hiw [exon] X:15051858 -> <- 1/268/335/5070 GYPSY
MICROPIA [LTR] 476 -> <- 3L:12165277 Rh7 [3'UTR]
For full list, see Supplementary Table 5
C
Chimeric mRNA molecules in >1 replicate
Number of chimeric reads detected
1000
100
10
1
1
10
100
1000
10000
100000
Combined expression level
FDR: < 0.1%
transposons
IGE set 1
IGE set 2
IGE set 3
IGE set 4
IGE set 5
IGE set 6
IGE set 7
IGE set 8
IGE set 9
IGE set 10

Figure 4

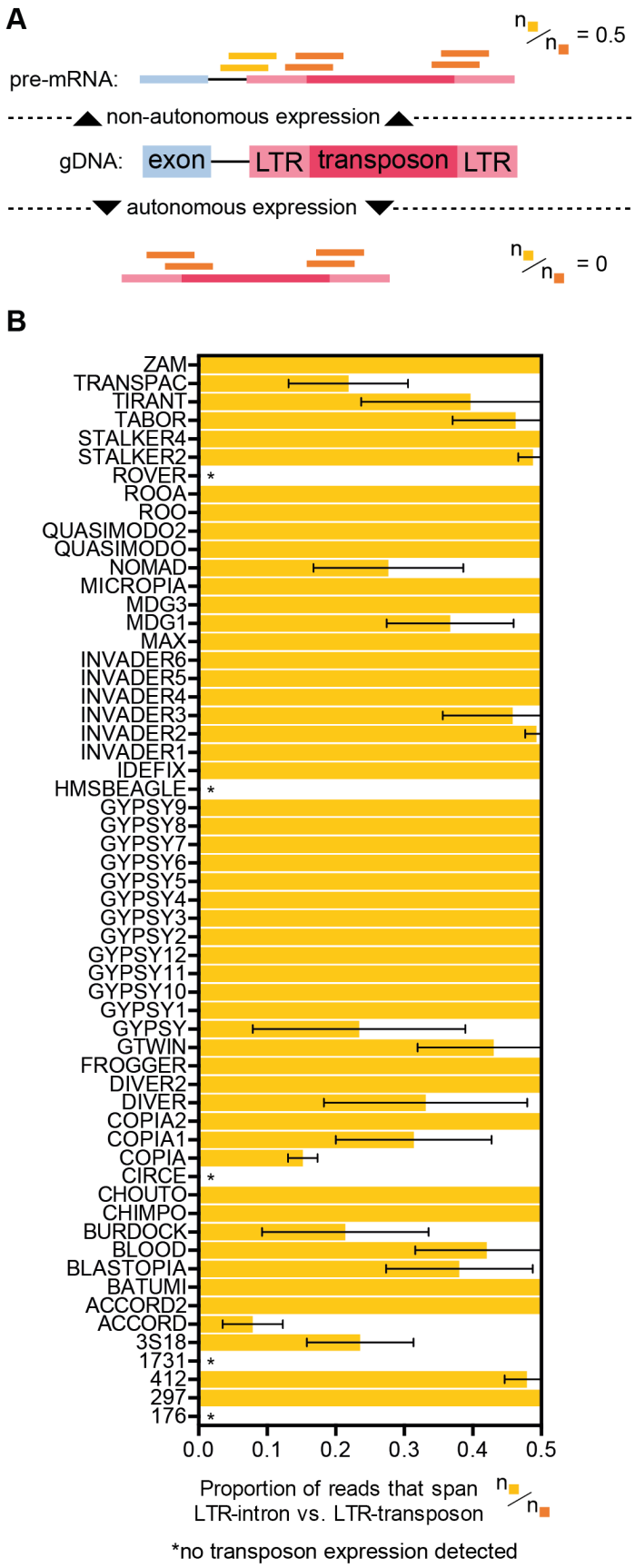
A
n / n = 0.5
pre-mRNA:
non-autonomous expression
gDNA:
exon
LTR
transposon
LTR
autonomous expression
n / n = 0
B
ZAM
TRANSPAC
TIRANT
TABOR
STALKER4
STALKER2
ROVER
ROOA
ROO
QUASIMODO2
QUASIMODO
NOMAD
MICROPIA
MDG3
MDG1
MAX
INVADER6
INVADER5
INVADER4
INVADER3
INVADER2
INVADER1
IDEFIX
HMSBEAGLE
GYPSY9
GYPSY8
GYPSY7
GYPSY6
GYPSY5
GYPSY4
GYPSY3
GYPSY2
GYPSY12
GYPSY11
GYPSY10
GYPSY1
GYPSY
GTWIN
FROGGER
DIVER2
DIVER
COPIA2
COPIA1
COPIA
CIRCE
CHOUTO
CHIMPO
BURDOCK
BLOOD
BLASTOPIA
BATUMI
ACCORD2
ACCORD
3S18
1731
412
297
176
0.0
0.1
0.2
0.3
0.4
0.5
Proportion of reads that span LTR-intron vs. LTR-transposon
n / n
*no transposon expression detected

Figure 4 - figure supplement 1

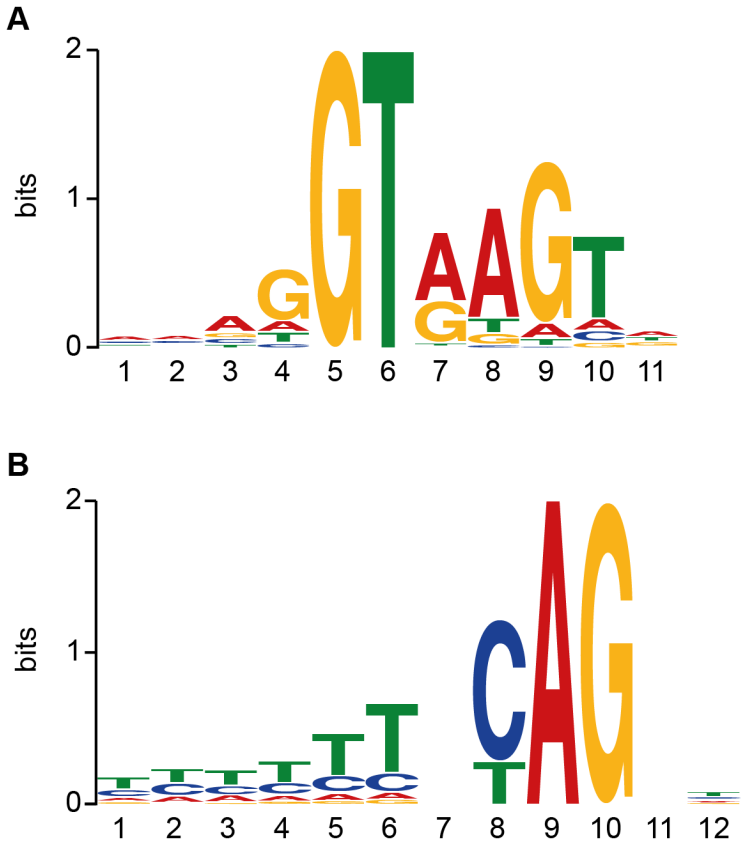

795

796

Figure 5

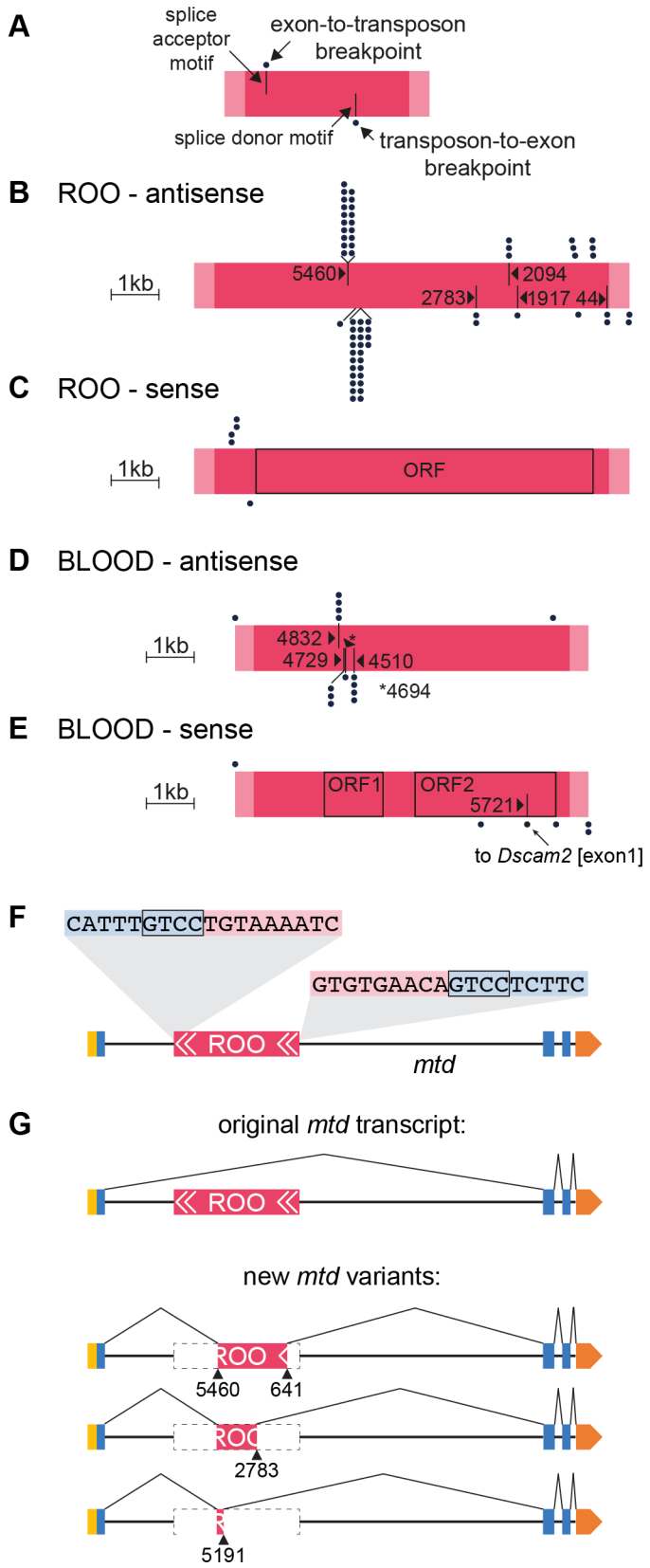
A
splice acceptor motif
exon-to-transposon breakpoint
splice donor motif
transposon-to-exon breakpoint
B ROO - antisense
1kb
5460
2094
2783
1917 44
C ROO - sense
1kb
ORF
D BLOOD - antisense
1kb
4832
4729
4510
*4694
E BLOOD - sense
1kb
ORF1
ORF2
5721
to Dscam2 [exon1]
F
CATTTGTCCTGTAAAATC
GTGTGAACAGTCCTCTTC
ROO
mtd
G
original mtd transcript:
ROO
new mtd variants:
ROO
5460
641
ROO
2783
5191

Figure 5 - figure supplement 1

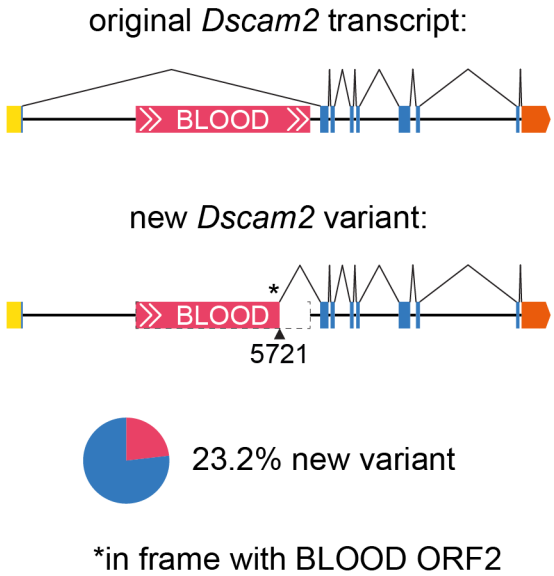

799

800

Figure 5 - figure supplement 2

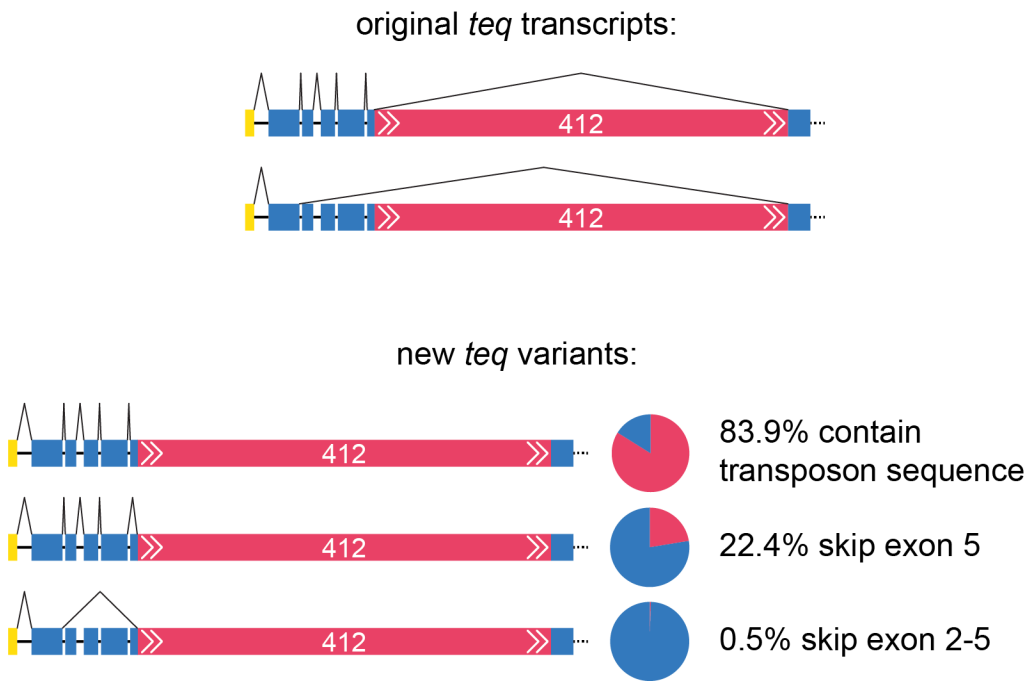

801

802

Figure 5 - figure supplement 3

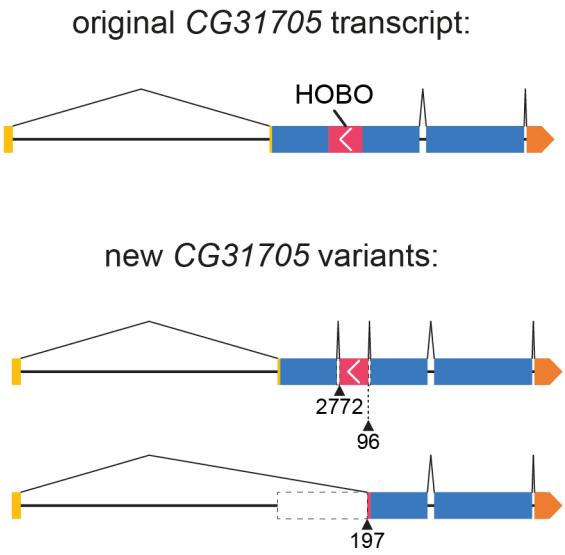

803

804

Figure 5 - figure supplement 4

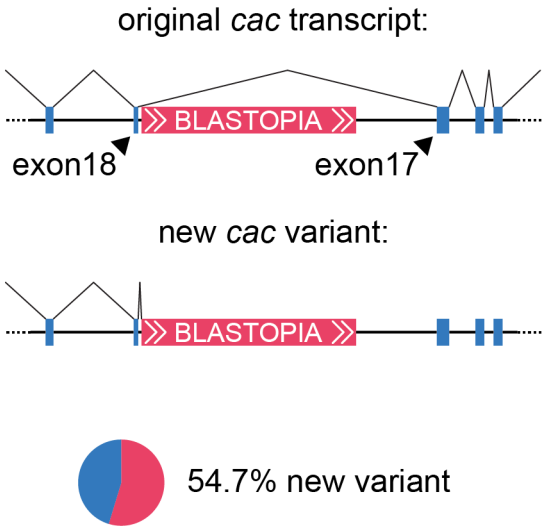

805

806

Figure 5 - figure supplement 5

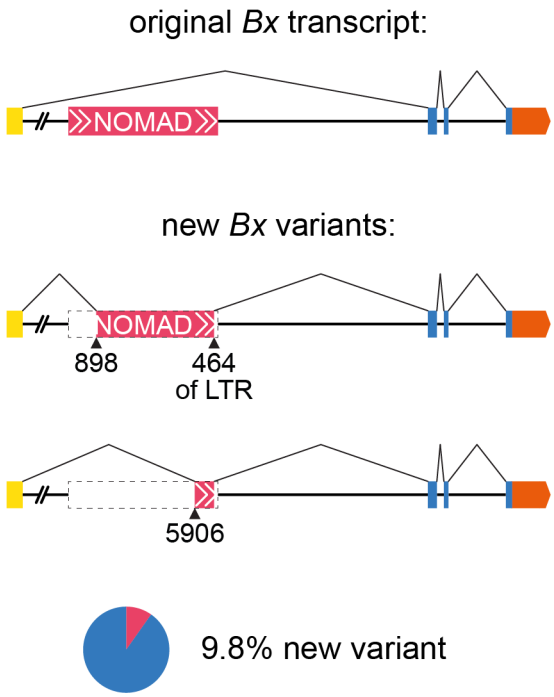

807

808

Figure 6

A

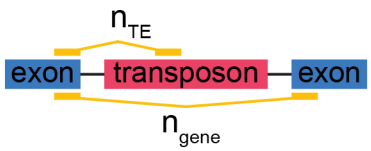

B

Gene	Transposon	$\frac{n_{TE}}{n_{TE}+n_{gene}}$
AstA-R1	NEG-ROO	100.0%
Pzl	I	100.0%
nAChRalpha1	NEG-DOC6	100.0%
Mec2	TRANSPAC	100.0%
Thd1	MAX	100.0%
CR45197	NEG-GYPSY	100.0%
CG45263	NEG-POGO	100.0%
Mocs1	P-ELEMENT	100.0%
AstC-R1	NEG-FW	94.1%
teq	412	83.9%
Cyp4p2	COPIA	80.4%

(for full list, see Supplementary Table 7)

809